Measurement Science
and Technology

PURPOSE-LED
PUBLISHING™

PAPER • **OPEN ACCESS**

Pressure-based indirect sensing of torch angular position in hand-held laser welding

To cite this article: Deniz Kaya *et al* 2026 *Meas. Sci. Technol.* **37** 465901

View the article online for updates and enhancements.



This content was downloaded from IP address 194.27.118.1 on 27/11/2026 at 22:14

Measurement Science and Technology

Check for updates

PAPER

OPEN ACCESS

RECEIVED
26 August 2026

ACCEPTED FOR PUBLICATION
3 November 2026

PUBLISHED
17 November 2026

Original content from this work may be used under the terms of the Creative Commons Attribution 4.0 licence.

Any further distribution of this work must maintain attribution to the author(s) and the title of the work, journal citation and DOI.

Pressure-based indirect sensing of torch angular position in hand-held laser welding

Deniz Kaya[1], **Mustafa K. İşman**[2], **Ebubekir Beyazoğlu**[1] and **Murat Reis**[1,*]

[1] Department of Mechanical Engineering, Bursa Uludağ University, Görükle Campus, 16059 Bursa, Turkey
[2] Şahterm Elektrikli Isıtıcılar San. ve Tic. A.Ş., Bursa, Turkey
[*] Author to whom any correspondence should be addressed.

E-mail: reis@uludag.edu.tr

Keywords: hand-held laser welding, angular positioning, shielding gas, process monitoring, operator error

Abstract

Hand-held laser welding offers high flexibility and speed, but limited repeatability due to its strong dependence on a consistent torch-to-surface-normal angle. This is critical in precision applications such as electric vehicle battery repair, where improper positioning compromises joint integrity. This study introduces a sensor-based method to indirectly monitor the torch holding angle (θ) by measuring shielding gas pressure inside the torch near the nozzle outlet, building upon a mechanical design described in a patent application whose underlying pressure-angle relationship is quantified here. Numerical simulations demonstrate that gas pressure varies monotonically with θ and remains independent of axial rotation (β). Experiments conducted across four flow rates (15–30 l min^{-1}) and six torch angles (15°–60°) establish that a 5° angular deviation yields a pressure change of approximately 4 kPa at 30 l min^{-1}. This corresponds to a theoretical resolution of 0.5° and suggests the potential for a monitoring resolution of ∼1° under the tested conditions. Empirical transfer functions derived across these flow rates provide a robust, closed-form foundation for real-time operator feedback systems in advanced manufacturing environments.

Nomenclature

Symbol	Description	Unit
θ	Angle between the torch and the surface normal	°
θ_{correct}	Intended (correct) torch-holding angle	°
θ_{wrong}	Actual (incorrect) torch-holding angle held by the operator	°
θ_{measured}	Torch angle estimated from the pressure-based sensing method	°
$\theta_{\text{threshold}}$	Operator-alert threshold angle (configurable)	°
$\Delta\theta_{\text{error}}$	Angular deviation between θ_{measured} and θ_{correct}	°
β	Rotational position of the torch about the laser beam axis	°
ΔP	Pressure difference relative to the reference position ($\theta = 90°$)	kPa
ΔP_{min}	Minimum resolvable pressure change of the sensing chain	kPa
e	Length of the movable nozzle segment	mm
d	Diameter of the nozzle	mm
Δe	Displacement of the laser beam focal point	mm
Q_{in}	Volumetric shielding gas flow rate at the torch inlet	l min^{-1}
$\dot{m}_{\text{in}}$	Mass flow rate at the torch inlet	kg s^{-1}
P_{out}	Gauge pressure prescribed at the pressure-outlet boundaries	Pa
S_{sensor}	Sensitivity of the MPXH6400A pressure sensor	mV kPa^{-1}
S_{sys}	Empirical system sensitivity (pressure change per degree of torch angle)	kPa/°
V_{ref}	Reference voltage of the analog-to-digital converter (ADC)	V

(Continued.)

© 2026 The Author(s). Published by IOP Publishing Ltd

(Continued.)

n_{ADC}	Resolution of the analog-to-digital converter	bit
ΔV_{min}	Minimum resolvable ADC voltage step	mV
$\Delta\theta_{min}$	Theoretical minimum resolvable angular change	°
V_{FSS}	Full-scale span voltage of the pressure sensor	V
R^2	Coefficient of determination of the fitted transfer function	—
RMSE	Root mean square error of the fitted transfer function	°

1. Introduction

Indirect, proxy-based sensing is a recurring strategy in measurement science whenever direct instrumentation is impractical due to space, access, or environmental constraints. Hand-held laser welding torch angular positioning, examined throughout this study, is one such case.

Hand-held laser welding is an increasingly widespread application in the automotive, aerospace, and sheet metal industries [1, 2]. Its potential is particularly high for delicate manual interventions in precision component repair. However, to fully realize this potential, auxiliary systems are required to minimize laser beam positioning errors. Industrial robotic arms allow for the precise manipulation of the laser beam required for advanced thermal management techniques [3]. By contrast, hand-held systems introduce operator-dependent angular positioning errors that can benefit from real-time monitoring. Process monitoring cameras and support systems, such as roller devices, have been developed to stabilize the welding geometry, improve ergonomics, and guide novice operators [4–6].

The torch-to-surface-normal angle is a critical operational variable that directly dictates weld pool geometry and joint integrity. It has been confirmed both experimentally and by simulation that variations in the angle of incidence produce significantly different weld cross sections. For instance, Madrid *et al* demonstrated these variations by keeping the gas flow rate and laser focus constant while altering the laser beam angle [7]. In manual operations, this angle is entirely under the operator's control, and even small deviations have been linked to focusing-tolerance limitations [8] and increased porosity in filler-welded joints [9]. Studies have identified critical angle thresholds for desired weld appearances [10] and established strong correlations between the incidence angle and penetration depth [11, 12]. The angle also differentiates the heating and cooling cycles, affecting microstructural transformations [13], and alters the weld pool volume in spot welding applications [14]. Torch angle has also been used as an input variable in neural network models for predicting weld geometry [15].

Because the shielding gas exits through the same nozzle opening, whose geometry is defined by the torch angle, the two are not independent phenomena: the gas pressure field is, in principle, a readable proxy for the torch angle. Before this coupling can be exploited for sensing purposes, however, it is necessary to understand how the shielding gas itself governs weld quality.

Beyond providing a protective atmosphere, the fluid dynamics of the shielding gas strongly influence weld quality, at times rivaling the laser parameters themselves [16, 17]. Measurements of the pressure and flow fields generated by the shielding gas have shown that irregular flow increases spatter formation, and that monitoring the exit pressure profile can be used to characterize nozzle performance and reduce oxidation and gas consumption [18–20]—a precedent that directly motivates the pressure-based sensing approach adopted in this work.

The gas flow serves two primary functions: protecting the weld pool from oxidation [21, 22] and shielding the optical system from spatter contamination [23–25]. Its performance depends on factors such as gas type, flow rate, delivery geometry, and nozzle design, which have been extensively studied in the broader welding literature [26–40].

Mechanistically, the flow and pressure characteristics of this shielding gas are geometrically coupled to the operator's grip. Any deviation in the torch-to-surface-normal angle physically expands or constricts the annular gap between the nozzle tip and the workpiece. This geometric restriction creates a measurable flow resistance and backpressure within the torch cavity, establishing a direct physical link between the internal gas pressure and the external holding angle.

It is important to clarify the distinction between the scope of the present study and that of the associated patent [41]. The patent primarily covers the mechanical architecture of the hand-held torch, including the adjustable nozzle geometry and the mechanism used for automatic focal-length compensation. These features are related to the design and operation of the torch itself. While the patent application describes using the shielding-gas pressure inside the torch to estimate the nozzle angle, it does not

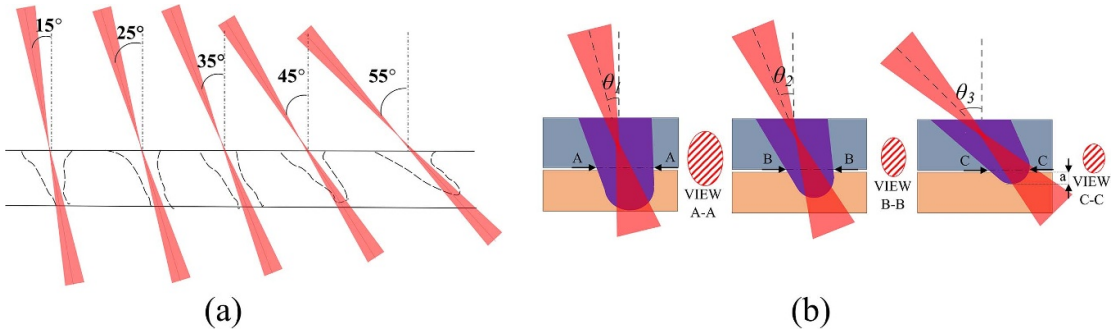


Figure 1. The effect of the torch-to-surface-normal angle (θ) on weld characteristics: (a) representative images of weld pool geometries formed at different incident angles, and (b) demonstration of the corresponding change in penetration depth during laser spot welding of thin sheet metal surfaces [4].

provide the numerical and experimental characterization or the calibrated pressure-angle transfer functions presented in this study. Establishing such a relationship requires dedicated numerical and experimental investigation. In this study, the pressure-angle relationship is therefore characterized through numerical simulations and experiments over a practical range of flow rates and torch angles. Based on these results, transfer functions are developed and the achievable angular resolution is evaluated, providing a basis for real-time torch angle estimation. The resulting methodology is not limited to the specific mechanism described in the patent application and can, in principle, be applied to other hand-held torch geometries with a comparable nozzle-to-surface gas-exit configuration.

Alternative sensing approaches, such as digital protractors [4, 5], require an extra pre-weld measurement step, while IMU (inertial measurement unit) or vision-based systems add significant hardware complexity. Despite these options, to the best of the authors' knowledge, no prior study has quantitatively established this pressure-angle relationship for hand-held laser welding torches, nor characterized its dependence on shielding gas flow rate or its achievable angular resolution—the central novel contributions of the present work. This research introduces a pneumatic control methodology to assist operators in maintaining the correct torch orientation. The physical architecture of the proposed device is currently patent-pending [41]. This paper provides the necessary scientific investigation of its operational mechanics. By integrating numerical flow simulations with experimental data, this work establishes the empirical transfer functions that provide a basis for future real-time error detection in industrial applications.

2. System development

The proposed system combines an absolute pressure sensor, an empirical transfer function, and a real-time feedback interface to monitor the torch angle. Among the various operator-controlled parameters, the torch-to-surface-normal angle (θ) is particularly difficult to control and can significantly affect weld geometry and mechanical properties [42].

As shown in figure 1(a), increasing the angle between the laser beam and the surface normal alters the weld pool geometry, resulting in reduced penetration depth and weld strength [4]. This effect is particularly important in precision spot welding of thin sheets, where sufficient penetration is required for joint strength, while excessive penetration into the underlying layer can damage the joined components. Figure 1(b) illustrates the resulting changes in weld penetration and cross-sectional geometry with welding angle. Recent experimental studies on hand-held laser welding have also shown that deviations in torch inclination alter the effective beam area and consequently affect the resulting weld penetration depth [43].

In addition to its effect on weld pool geometry, the torch-to-surface-normal angle at which the laser light falls on the welding surface may also affect the reflectivity of the laser [44]. Beyond reflectivity, angular deviations inherently shift the position of the laser focal point, either above the surface or deeper into the material (figure 2). As geometrically detailed in figure 3 and derived from the nozzle geometry described in the patent application [41], the focal point displacement ($|\Delta e|$) caused by a holding error can be calculated using equation (1), where d is the nozzle diameter,

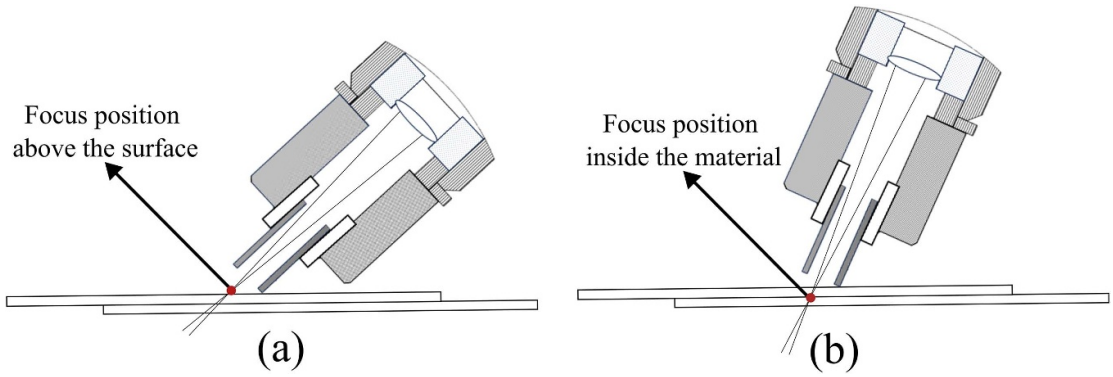


Figure 2. Change of laser focal spot position with change of the welding torch-to-surface-normal angle [41].

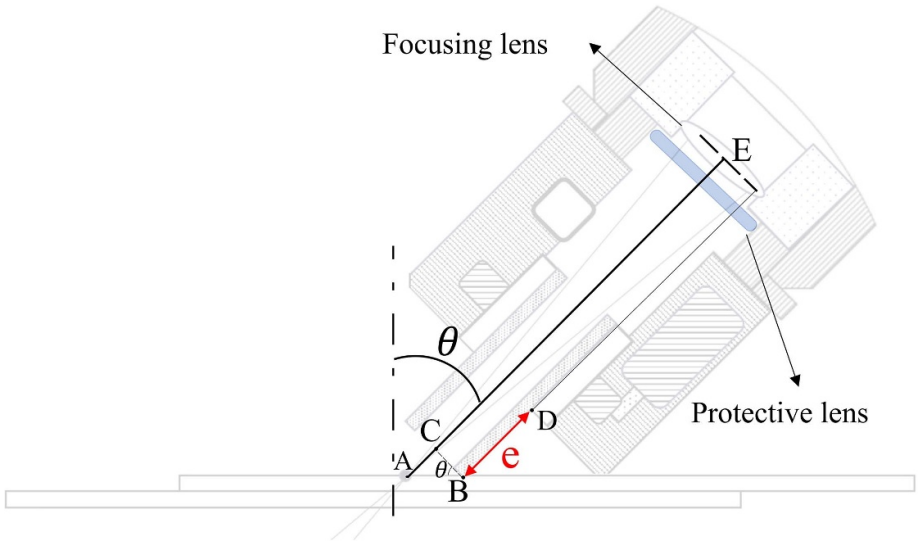


Figure 3. Geometric representation for calculating the displacement of the focal spot position depending on the welding torch holding angle, where *e* represents the length of the movable nozzle segment.

and θ_{correct} and θ_{wrong} represent the intended and actual torch-to-surface-normal angles, respectively.

$$|\Delta e| = \left| \frac{d}{2} \left(\tan\theta_{\text{correct}} - \tan\theta_{\text{wrong}} \right) \right|. \tag{1}$$

As demonstrated by this geometric relationship and further illustrated in figure 4, the focal deviation $|\Delta e|$ scales proportionally with the nozzle diameter for any given angular error. To maintain a consistent focal spot during manual welding, this physical shift must be continuously compensated. While a separate mechanism described in patent application [41] has been developed by the authors to physically adjust the nozzle length for this compensation, the pressure-based sensing method presented in this current study is designed to supply the critical real-time angular measurement required to drive such a system.

Beyond its effect on the focal point, the torch-to-surface angle also governs the geometry through which the shielding gas exits the nozzle. As illustrated in figures 5(a) and (b), the gap between the cylindrical nozzle and the weld surface acts as a partially obstructed annular outlet. When the torch is held at steep angles like in figure 5(a) (lower θ), this physical clearance decreases, reducing the effective flow area and hydraulic diameter. This geometric constriction increases flow resistance and produces a measurable rise in pressure within the torch cavity. Conversely, in figure 5(b) at more inclined angles (higher θ), the effective flow area expands, allowing the gas to exit the system easily with minimal resistance. Smooth gas flow without flow separation, turbulence, or backflow is crucial, as it creates a stable aerodynamic barrier that prevents slag spatter from entering the nozzle. Contamination on the protective lens from weld spatter can scatter or absorb laser radiation, which significantly alters the focal shift and

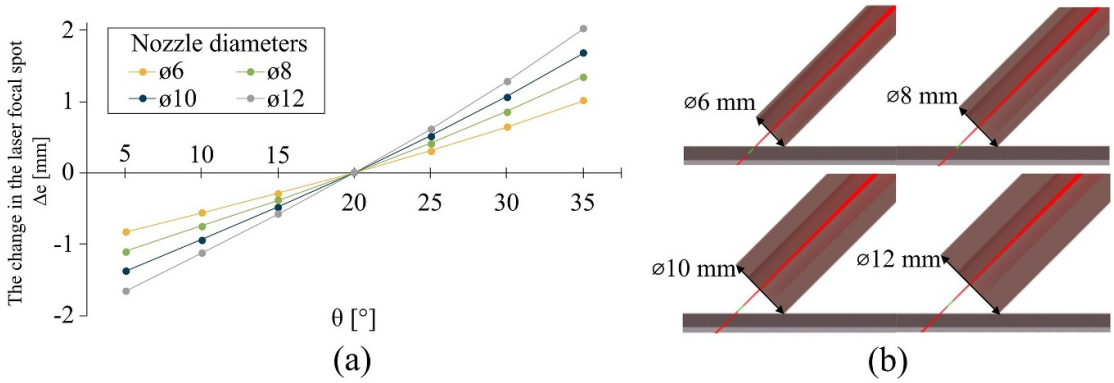


Figure 4. (a) The change in the laser focal spot due to torch holding errors for different nozzle diameters, Δe. (b) Schematic illustration of the effect of nozzle diameter on focal displacement.

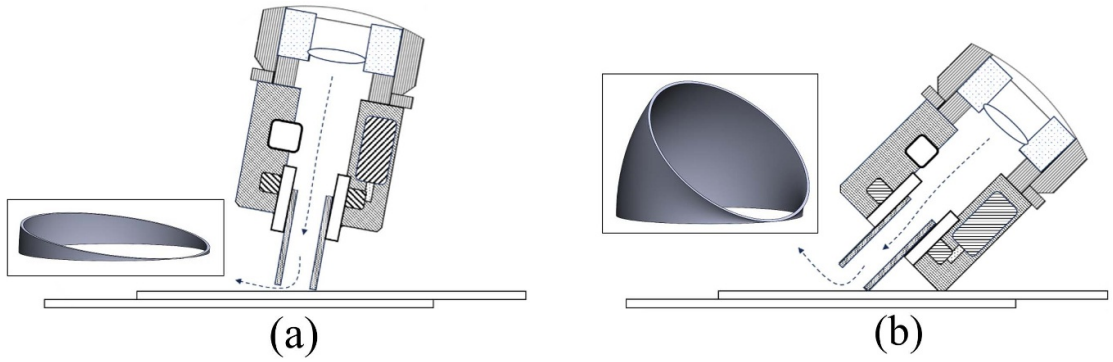


Figure 5. Gas outlet cross-sections at different welding torch holding angles (a) steep torch orientation (lower θ) and (b) inclined torch orientation (higher θ) [41].

power density distribution of the beam [45]. Therefore, monitoring this pressure-angle relationship ensures proper joint geometry and directly aids in optimizing gas consumption and improving overall process costs.

The operating logic of the proposed system, combining the pressure-based angle estimation with both the continuous focus-adjustment mechanism and the threshold-gated operator-alert function, is summarized in figure 6.

As shown in process flow chart figure 6, the estimated torch angle θ_{measured} feeds two parallel functions. The nozzle-stroke computation and the subsequent drive of the focus-adjustment motor operate continuously and unconditionally on every measurement cycle. This logic is consistent with the focus-compensation mechanism described in the patent application [41], which is designed to physically maintain the focal point regardless of the instantaneous grip angle. In contrast, the operator-alert branch is triggered only when the estimated angular deviation $|\Delta\theta_{\text{error}}|$ exceeds a configurable threshold $\theta_{\text{threshold}}$. This threshold is deliberately set with a safety margin above the theoretical minimum resolvable angle $\Delta\theta_{\text{min}} \approx 0.5°$ derived in section 5.1. A practical value of $\theta_{\text{threshold}} \approx 1°–2°$ is suggested, though this can be tuned according to the precision requirements and tolerance of the target welding application. The continuous focus-compensation logic operates as a core element of the mechanism described in the patent application [41]. On the other hand, the threshold-gated operator-alert function serves as a distinct design feature specific to the monitoring system presented in this study. In a practical scenario, the shielding gas pre-flow initiates just before the laser is fired. This allows the system to instantaneously verify the operator's initial holding angle and issue any necessary alerts before the actual weld is triggered. Consequently, the method could help detect positional errors before welding begins.

Minimizing the operator's angular positioning errors requires a dedicated feedback system. Such a semi-automatic feedback mechanism could improve process consistency and potentially reduce operator-related errors and rework.

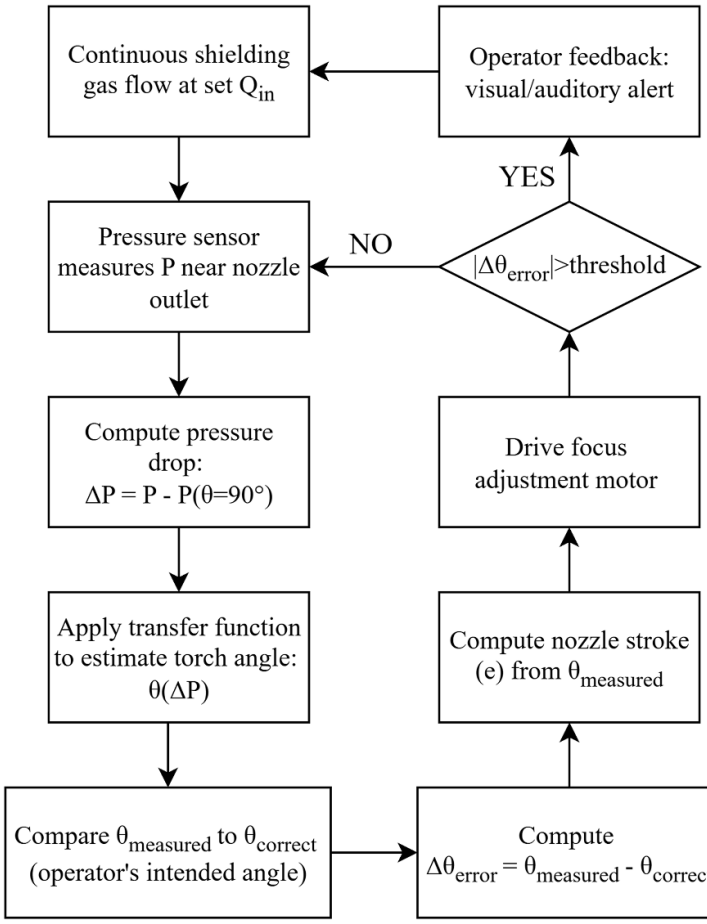


Figure 6. Flowchart of the proposed closed-loop system combining continuous focus adjustment and threshold-based operator alerts.

3. Numerical simulation

3.1. Computational setup

The numerical model does not aim to simulate the operator's hand-held welding motion or torch trajectory. Instead, it calculates the shielding-gas flow for a fixed torch position defined by the angle θ and rotation β. In this way, the CFD model is independent of the operator and focuses only on the flow behavior for a given torch position. The effect of human factors, such as the angles an operator can realistically hold and the variation between measurements, is considered experimentally using six different angles and four repetitions for each condition (section 4).

In the numerical model, the shielding gas flow is assumed to be isothermal and incompressible. Although the actual welding process involves high temperatures, this assumption is considered reasonable for the proposed sensing method for two main reasons. First, the initial angle verification is mainly performed during the pre-flow stage, before the laser is activated, when the gas remains close to ambient temperature. Second, during welding, the pressure sensor is located relatively far from the weld pool, just before the protective lens. The continuous flow of fresh shielding gas limits heat transfer from the weld pool to the internal nozzle cavity. Therefore, the gas density and flow behavior inside the nozzle are expected to be only minimally affected by the weld heat, making the isothermal assumption sufficient for evaluating the pressure-angle relationship.

It is important to note that the numerical and experimental campaigns in this study were carried out with different but complementary objectives. The fixed and variable parameters used in each campaign are summarized in table 1. The numerical model was first used to establish the qualitative basis of the proposed sensing approach before conducting the experiments. In particular, the simulations were used to verify that the pressure changes monotonically with θ and remains insensitive to β. The experimental campaign was then conducted over a wider angular range and at different flow rates to quantitatively characterize the pressure-angle relationship and derive the transfer functions presented in section 4. This

Table 1. Test conditions and objectives of the numerical and experimental campaigns.

Parameter	Numerical (CFD)	Experimental
Gas type	Argon	Argon
Nozzle inner diameter	7 mm	7 mm
Gas flow rate	30 l min^{-1}	15, 20, 25, 30 l min^{-1}
Torch angle (θ)	15°, 20°, 25°, 30°	15°, 20°, 25°, 30°, 45°, 60°
Torch rotation (β)	0°–360° (Variable)	Fixed
Repetitions	1 (Steady-state)	4 per condition
Primary purpose	Qualitative verification: direction of the θ–pressure relationship and β-independence	Quantitative transfer-function derivation for real-time angle estimation

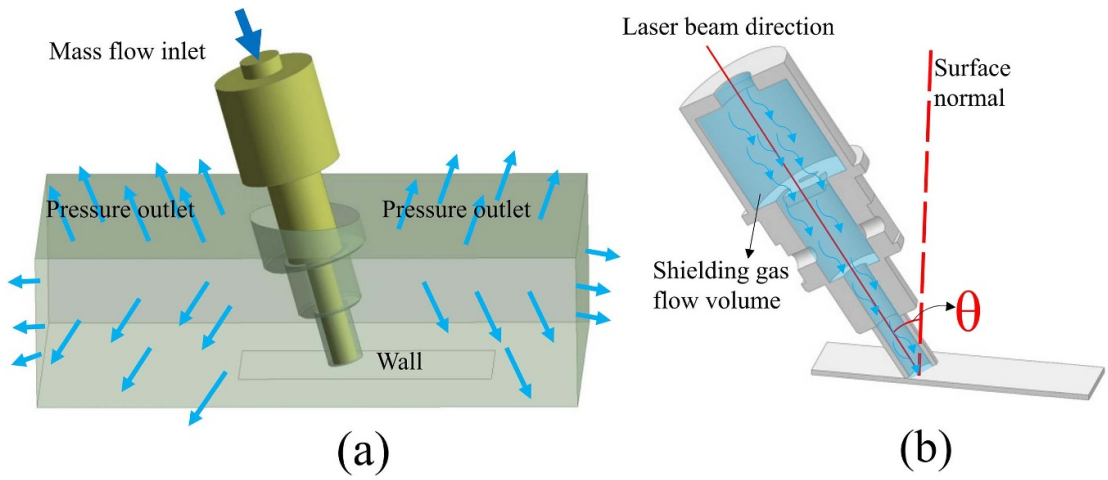


Figure 7. Boundary conditions for finite volume model of welding torch shielding gas flow (a) and schematic representation of process (b).

distinction explains the differences in the scope of the two campaigns, particularly in terms of flow rate and angular range.

The CFD analysis was limited to a single flow rate of 30 l min^{-1}. The experiments in section 4 showed the highest sensitivity to pressure changes caused by angular error. This provides a demanding case for checking the pressure-angle relationship. Since the same trend was subsequently confirmed experimentally at all four flow rates, a full CFD analysis for all flow rates was not considered necessary.

It should be emphasized that the numerical campaign was not designed to reproduce the absolute experimental pressure values, nor to serve as a direct quantitative validation benchmark for the experimental transfer functions. Its purpose is twofold and strictly qualitative: first, to verify that the sensor reading is insensitive to the torch's rotational position (β) about the laser beam axis, so that the sensor can be mounted at any convenient azimuthal position without affecting measurement accuracy; and second, to confirm that a change in the torch-to-surface-normal angle (θ) produces a measurable, monotonic pressure difference at the sensor location, independent of the specific magnitude of that difference. The simplified computational domain does not capture pneumatic fittings, connector losses, or other secondary flow resistances present in the physical test rig, and a one-to-one numerical-experimental pressure comparison is therefore neither expected nor pursued.

The computational domain and its boundary conditions are shown in figure 7(a), while the torch-to-surface-normal angle (θ) is defined in figure 7(b). A constant flow rate of 30 l min^{-1} (i.e. $\dot{m}_{\text{in}} = 8.92 \times 10^{-4}$ kg s^{-1}) was prescribed at the torch inlet as a mass-flow inlet. All outer boundaries of the surrounding domain were set as pressure outlets at atmospheric pressure ($P_{\text{out}} = 0$ Pa gage), and all solid surfaces were treated as no-slip walls.

The SST k-ω turbulence model was used, as it provides a more reliable prediction of near-wall velocity gradients and flow separation in impinging jet-type flows than standard k-ε formulations [46]. Nozzle geometry and shielding gas coverage have similarly been shown to significantly affect flow behavior in related gas-shielded welding processes [47].

The domain was discretized with a polyhedral mesh, refined with prismatic boundary-layer elements near the walls and around the nozzle exit and sensor location. To adequately resolve the viscous sublayer

Table 2. Mesh independence study results based on the pressure sensor location.

Mesh level	Number of elements	Relative difference (%)
Coarse	0.5×10^6	—
Medium	1.2×10^6	4.6[a]
Fine	2.3×10^6	< 1.5[b]

[a]Relative to the Coarse mesh.
[b]Relative to the Medium mesh.

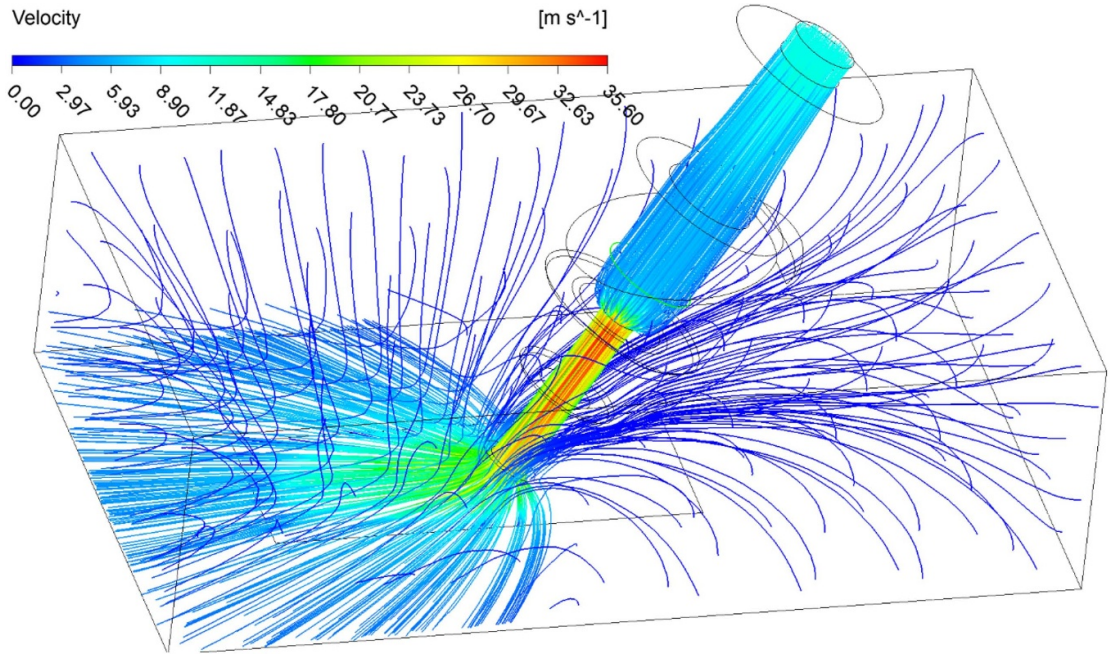


Figure 8. CFD-predicted gas velocity streamlines (30 l min^{-1}, $\theta = 20°$) demonstrating flow acceleration up to 35.6 m s^{-1} due to the geometric constriction at the nozzle outlet.

as required by the SST k-ω turbulence model, these inflation layers were designed to maintain an average wall y^+ value of ≈ 1 at the critical nozzle exit and internal cavity walls. A grid-independence study using three mesh densities (table 2) showed that the static pressure at the sensor location changed by less than 1.5% between the medium and fine meshes; the medium mesh (1.2×10^6 elements) was therefore used for all subsequent analyses. The governing equations were solved with a steady-state, pressure-based solver (SIMPLE scheme, second-order upwind discretization), and the solution was considered converged once the scaled residuals fell below 10^{-6}.

3.2. Flow characteristics

Representative gas streamlines obtained from the numerical simulations are depicted in figure 8. The shielding gas accelerates through the converging section of the nozzle, reaching its maximum velocity at the nozzle exit, where the cross-sectional area is smallest, confirming that the model reproduces the expected flow behavior inside the welding torch.

The static pressure at the sensor location varied significantly with the torch-to-surface-normal angle. To assess whether the operator's ability to keep the sensor facing upward affects the reading, the pressure distribution around a circle passing through the sensor location was also calculated. The rotational position of the torch about the laser beam axis is defined by the angle β, as represented in figure 9(b). As shown in figure 9(a), the pressure variation over the full β range (0°–360°) is negligible, so the sensor reading is unaffected by the torch's rotational orientation. In contrast, the torch-to-surface-normal angle (θ) produces a pressure difference of 600 Pa within 15°–20° and 300 Pa within 20°–25°, meaning that a sensor with ∼100 Pa sensitivity can resolve angular changes of about 1°.

Consistent with the qualitative scope defined in section 3.1, the numerical results confirm that pressure varies monotonically with θ and the measurement is insensitive to β.

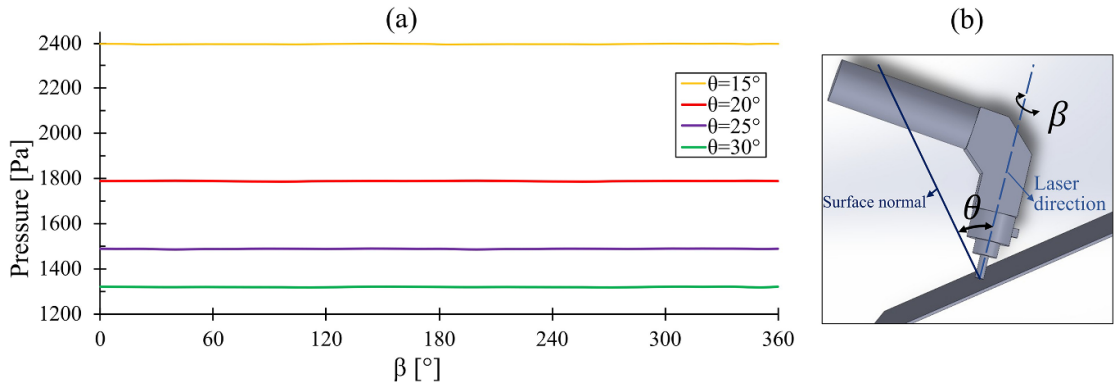


Figure 9. (a) Pressure change at sensor position in response to rotation of the laser beam around its axis (torch rotation around laser beam) for four different angles ($\theta = 15°$, 20°, 25°, and 30°) and (b) representation of θ and β angles.

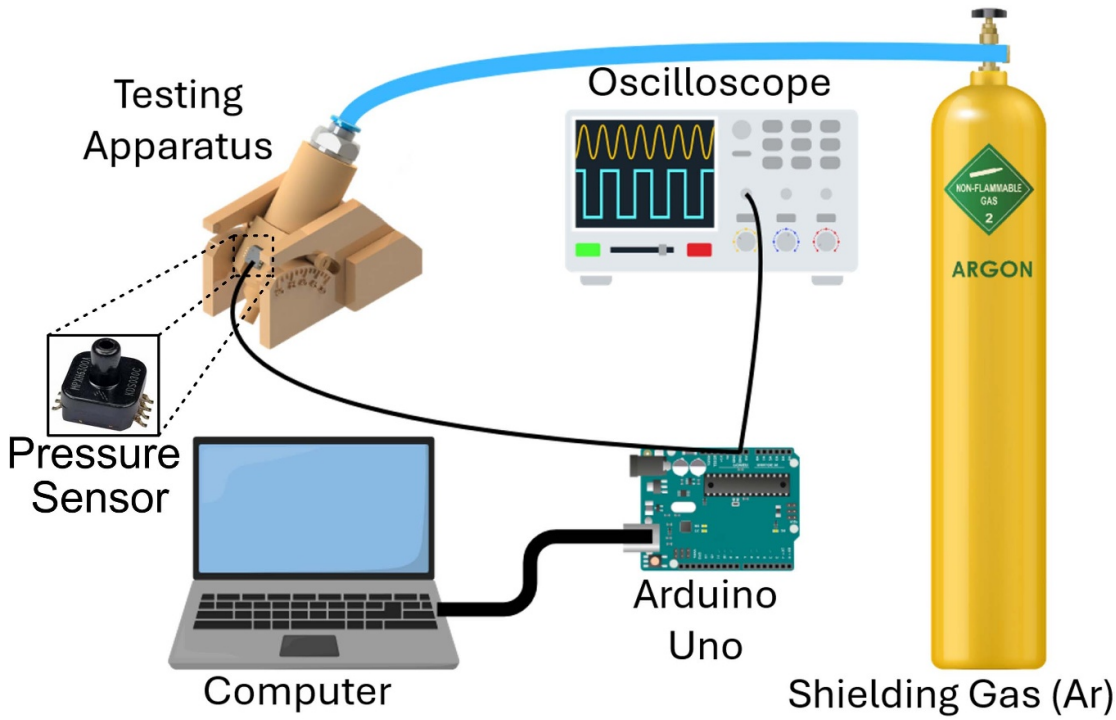


Figure 10. Overview of the test setup.

4. Experimental system

To quantitatively characterize the pressure-angle relationship, a dedicated experimental setup was built to reproduce and measure the shielding gas pressure response under controlled torch angles and flow rates. The overall test setup, comprising the testing apparatus, the argon gas supply, and the data acquisition chain, is shown in figure 10. Gas was discharged from the argon cylinder at the desired flow rate and delivered to the testing apparatus, where the pressure sensor output was recorded. The output voltage values obtained from the sensor were read comparatively via an oscilloscope, which provided a voltage measurement resolution of approximately 5 mV, and a computer's serial interface using an Arduino Uno data acquisition unit. The analog voltage readings were subsequently converted to absolute pressure values by applying the sensor's official sensitivity coefficient of 12.1 mV kPa^{-1}.

In the experiments, a simplified Laser ISSE brand manual laser welding torch model was created to simulate the gas flow inside a hand-held welding torch. This simplified model was also used in the numerical analysis studies. The simplified torch model focused on the section between the protective

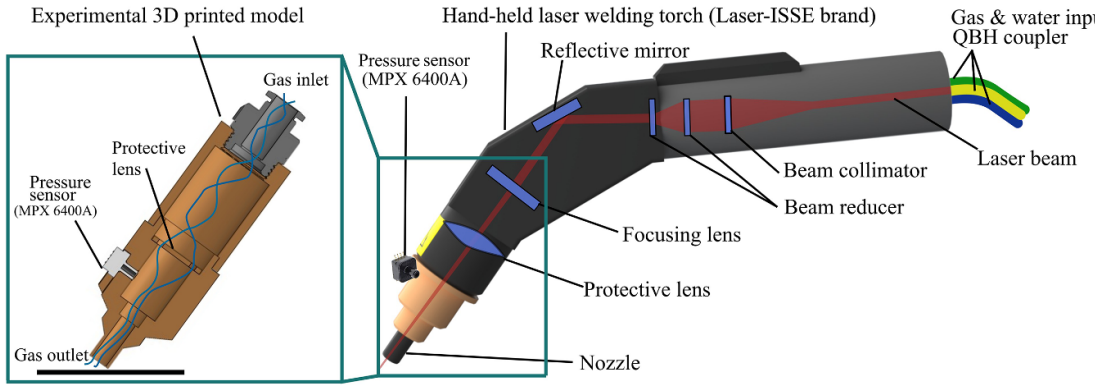


Figure 11. Cross-sectional schematic of the commercial Laser-ISSE hand-held torch (right) and the simplified 3D-printed experimental model (left) reproducing only the section between the protective lens and the exit nozzle used for the pressure measurements.

Table 3. Variables of the experiment.

Gas type	Argon
Nozzle inner diameter	ø7 mm
Gas flow rates (l min^{-1})	15, 20, 25, 30
Torch/surface normal angles	15°, 20°, 25°, 30°, 45°, 60°

lens and the exit nozzle, and a 3D model was produced only for this specific part of the torch. While the gas passing through the holes around the protective lens in the real hand-held welding torch moves toward the nozzle exit, these details were neglected in the simplified model both in the simulations and the experimental model. It was assumed that the protective gas entered the volume before the protective lens through a cylindrical opening. A nozzle inner diameter of 7 mm was selected for the experimental model. An absolute pressure sensor (NXP Semiconductors MPXH6400A) measuring 20–400 kPa was placed in the middle of the cylindrical volume just in front of the protective lens. The gas flow volume and the cross-sectional geometry of the torch model are shown in figure 11. Although the sensor is shown in the figure's upper part of the cylindrical volume section, numerical simulations have shown that the sensor at the top, bottom, or side has no significant effect on the pressure change (figure 9). This means the torch-to-surface-normal angle (θ) will be measured accurately even if the laser beam is held at different angular positions around its axis while the welding torch tip makes a certain angle with the surface. To adjust the angle of the experimental welding torch model relative to the surface normal, a linkage mechanism was designed that allows the torch holder to be rotated and locked at the six discrete angle positions listed in table 3, ensuring a fixed and repeatable angle during each measurement.

In the experiments, argon (Ar) was supplied to the system as the shielding gas at four different flow rates (15–30 l min^{-1}), selected to bracket the range commonly reported for shielding gas flow in industrial laser welding of metals, where flow rates of 10–30 l min^{-1} are typically used to balance weld pool protection and gas consumption. At flow rates of 15, 20, 25, and 30 l min^{-1} of argon, the torch model was positioned at the six angle values specified in table 3. Figure 12 shows the experimental torch model secured on the angle-adjustment platform at representative angular positions, illustrating the locking mechanism used to fix and repeat each measurement angle. Data were taken from the absolute pressure sensor placed on the torch at this time. The sensor provides an analog output between 0–5 V. The voltage values were read on the oscilloscope and the Arduino serial screen. The values between 0–5 V were converted to pressure values based on a linear function.

5. Results and discussion

The numerical analysis results showed that a 5° error in the torch-to-surface-normal angle produces a pressure change that can be measured with sufficient precision using the existing pressure sensor (NXP Semiconductors MPXH6400A). Consistent with the qualitative objective of the CFD campaign outlined in section 3.1 (table 1), the numerical results confirmed the same monotonic trend later quantified experimentally: static pressure at the sensor location increases as θ decreases. As established in

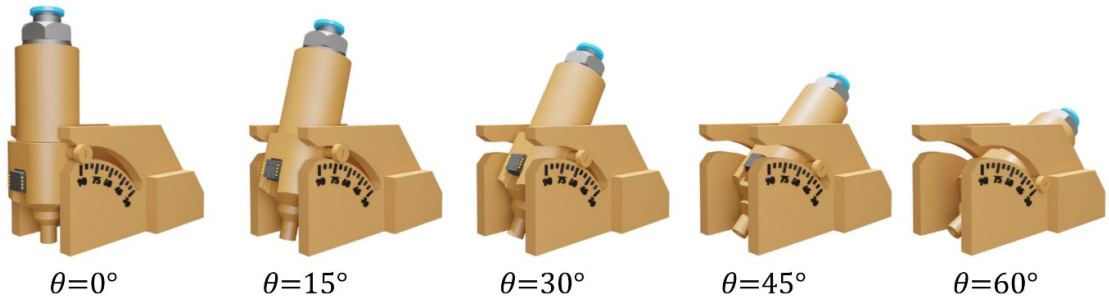


Figure 12. The experimental torch model secured on the angle-adjustment platform, shown at different angular positions (θ = 0°, 15°, 30°, 45°, and 60°).

section 3.1, the CFD campaign's role was qualitative rather than a quantitative validation benchmark. Based on this qualitative confirmation, the experimental analysis aims to determine the pressure changes that occur due to the cross-sectional narrowing at the torch tip at different holding angles and shielding gas flow rates. In this way, trend curves can be created by applying numerical analysis techniques to the results obtained, and functions that give the angular position depending on the pressure can be obtained. With the help of these functions embedded in the control software of the laser welding torch, this study establishes the theoretical and static functional basis for a system where the operator could monitor the relative angle between the welding torch and the weld surface normal through continuous pressure measurements. Since hand-held laser welding is highly susceptible to pore formation under suboptimal conditions, continuous monitoring of the shielding gas flow helps ensure the joint's mechanical integrity and microstructural quality [48]. The flow rates and torch angles tested (table 3) were chosen to reflect industrially relevant shielding gas conditions, with measurements concentrated near the vertical position, where angular precision has the greatest practical impact on weld quality, while still covering more oblique angles to capture the general trend.

Figure 13 shows the change of shielding gas pressure at the sensor position for four different shielding gas flow rates (15, 20, 25, and 30 $\mathrm{l\,min^{-1}}$) and six different torch-to-surface-normal angles (15°, 20°, 25°, 30°, 45°, and 60°). In particular, it is understood that at angles close to the vertical position (in the range of 15–20 degrees) and at a shielding gas flow rate of 30 $\mathrm{l\ min^{-1}}$, a 5° error in the welding torch holding angle causes a pressure difference of approximately 4 kPa at the sensor. This effect decreases as the shielding gas flow rate decreases. However, even at a shielding gas flow rate of 15 $\mathrm{l\ min^{-1}}$, a 5° position error in the range of 15–25 degrees creates a pressure difference of almost 2 kPa at the pressure sensor. It is understood from the curves that this significant effect of pressure change decreases at low flow rates of the shielding gas and at inclined angles of the welding torch (at large values of the angle between the welding torch and the normal of the welding surface). In practice, high gas flow will provide greater accuracy in determining the angle change during welding. Since the pressure signal becomes small at low flow rates and at angles between 30° and 45°, measuring the pressure change in this region accurately (approximately 50 Pa) is necessary. Otherwise, it may not always be possible to determine the angle value accurately due to fluctuations in the pressure value resulting from angular changes.

Detection of the faulty position of the welding torch and directing the operator to the correct holding angle is a process that must be done quickly and without delay. Rather than employing computationally heavy real-time root-finding algorithms for high-degree polynomial functions, this study models the pressure-angle relationship using single-term exponential decay functions (*ExpDec*1) fitted to the experimental data in figure 13. To provide a direct and efficient input for the torch control software, these exponential models were mathematically inverted. The resulting direct transfer functions, which express the torch holding angle explicitly as a logarithmic function of the measured pressure difference ($\theta = f(\Delta P)$), are presented in table 4. This mathematical inversion eliminates the computational latency associated with iterative root-finding, which is a necessary (though not by itself sufficient) condition for capturing instantaneous angular fluctuations in a future dynamic implementation. The experimental validations in this study were conducted exclusively under static holding conditions; no dynamic (continuously moving torch) experiments were performed, and all references to real-time operation in this manuscript describe the intended target application rather than a condition that has already been experimentally verified. Despite this limitation, the proposed methodology exhibits strong potential for dynamic, real-time monitoring. According to the manufacturer specifications, the MPXH6400A sensor features a rapid response time of 1ms. While the MPXH6400A sensor itself responds within 1 ms, the

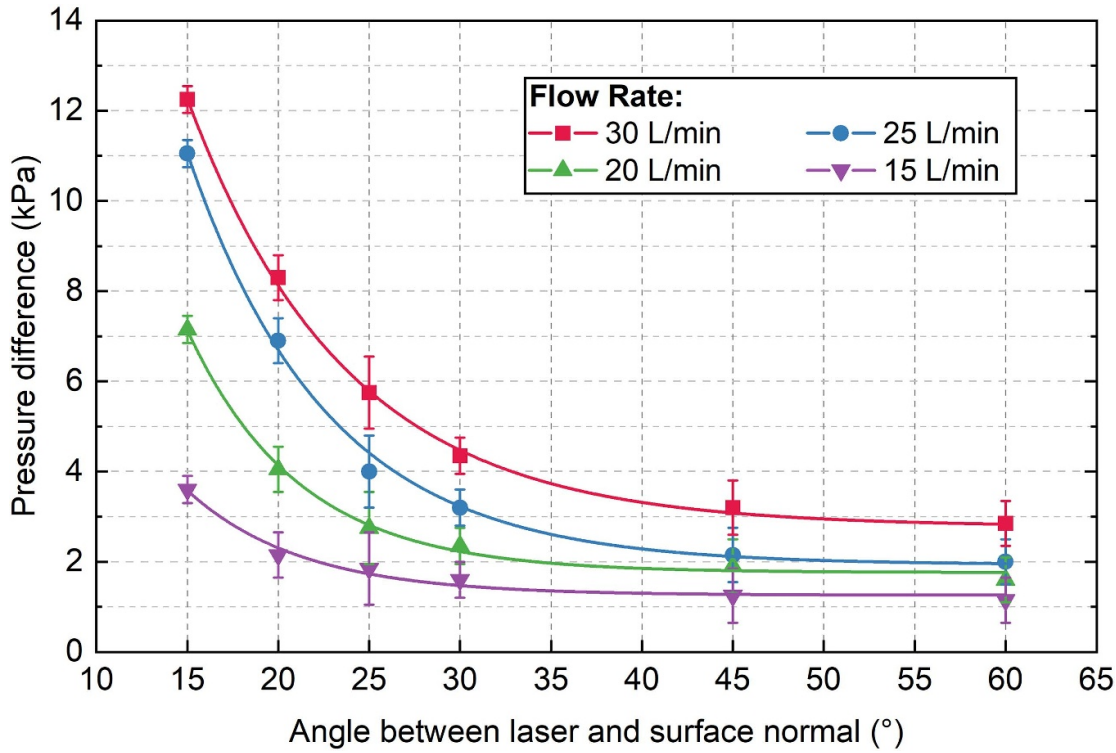


Figure 13. Measured shielding gas pressure variations across different flow rates and torch-to-surface-normal angles, including exponential fits.

total latency of the proposed detection chain also includes analog-to-digital conversion and control-logic evaluation. A typical 10–12 bit ADC on a low-cost microcontroller completes a single conversion in well under 1 ms (on the order of tens of microseconds for modern SAR-type converters), and evaluating the closed-form logarithmic transfer function (table 4) requires a single closed-form evaluation rather than an iterative search, adding negligible further delay. The estimated end-to-end latency of the sensing chain is therefore expected to remain on the order of a few milliseconds, well below the ∼100–300 ms range typical of human visual-motor reaction times—suggesting that the sensing chain itself would not be the bottleneck for operator feedback. This estimate does not, however, substitute for a direct measurement of the full closed-loop latency under dynamic conditions, which is left for future work (section 5.2).

The pressure difference (ΔP) reported in figure 13 is defined as the difference between the pressure measured at the sensor location and the pressure measured at $\theta = 90°$ (reference position, fully open nozzle cross-section).

The nozzle diameter (fixed at 7 mm in this study) and the shielding gas flow rate jointly determine the gas exit velocity, and consequently, the pressure sensitivity to angular error. For a smaller nozzle diameter, the same volumetric flow rate would produce higher exit velocities and a stronger pressure-angle relationship, whereas a larger diameter would reduce sensitivity. This trade-off should be considered when adapting the method to torches with different nozzle geometries. Measurements for each experimental condition (combination of shielding gas flow rate and torch-to-surface-normal angle) were repeated four times. The system was allowed to reach steady-state flow before recording the pressure data for each independent iteration.

These results are consistent with previous studies showing that shielding-gas pressure and flow fields are highly sensitive to small changes in nozzle geometry and stand-off conditions [18–20, 47]. The present study extends this understanding to the effect of torch-to-surface angle in a hand-held welding configuration and, to the authors' knowledge, is the first to establish quantitative transfer functions for this relationship. The monitoring resolution of approximately 1° estimated in this study is of the same order as that reported for IMU-based torch tracking systems, which typically show root-mean-square errors of 1°–3° [49, 50], although a direct performance comparison requires validation under equivalent conditions; for conventional manual jig-based measurements, errors of up to 5.26° have been reported [51]. Theoretical sensor-resolution calculations confirm a minimum resolvable angular change ($\Delta\theta_{\min}$) of approximately 0.5°, derived directly from the fundamental relationships governing the analog-to-digital conversion and sensor sensitivity [52]. In comparison with digital-protractor-based feedback

Table 4. Logarithmic transfer functions, R^2, and RMSE values for the tested gas flow rates.

Flow rate ($l\,min^{-1}$)	Transfer functions	R^2	RMSE (°)
30	$\theta_{30}(\Delta P) = -8.71 \cdot \ln\left(\frac{\Delta P - 2.78}{53.14}\right)$	0.999	0.99
25	$\theta_{25}(\Delta P) = -7.68 \cdot \ln\left(\frac{\Delta P - 1.93}{64.39}\right)$	0.999	0.99
20	$\theta_{20}(\Delta P) = -6.13 \cdot \ln\left(\frac{\Delta P - 1.76}{62.01}\right)$	0.998	0.99
15	$\theta_{15}(\Delta P) = -6.29 \cdot \ln\left(\frac{\Delta P - 1.26}{25.23}\right)$	0.991	0.98

systems [4, 5], the proposed approach also eliminates the need for additional angle-measuring hardware and pre-weld calibration.

The transfer functions given in table 4 are valid within the tested angular range of $15° - 60°$ and the flow-rate range of 15–30 $l\,min^{-1}$. Instead of using high-order polynomials that risk statistical overfitting and lack physical meaning, the exponential decay models and their mathematical inversions provide a robust representation of the fluid dynamics at the nozzle tip. This approach yields exceptional statistical reliability, with coefficient of determination (R^2) values exceeding 0.99 for all tested flow rates, indicating an excellent fit between the measured pressure differences and the predicted angular positions for real-time control applications.

The feedback system primarily monitors angular deviations. In addition to this control function, the base parameter driving the pneumatic sensing mechanism plays a dual role in process economics. Since the increasing gas flow rate raises the shielding gas velocity at the nozzle outlet, it creates a stronger aerodynamic resistance against slag particles approaching the lens, thereby reducing protective lens contamination and extending its replacement interval. At the same time, the shielding gas continues to protect the weld pool from oxidation regardless of flow rate. However, higher gas flow rates also increase operating costs. This introduces an inherent trade-off between shielding gas consumption and protective lens replacement expenses. Identifying the optimum flow rate that balances these two competing costs while maintaining adequate weld pool protection and the desired weld quality would require a dedicated cost model supported by extensive field data, and is therefore left outside the scope of the present study.

5.1. Error and resolution analysis for angular positioning

To assess the feasibility of a $\sim 1°$ monitoring resolution, the resolution of the pressure-sensing chain was evaluated based on the pressure sensor sensitivity and the quantization limit of the analog-to-digital conversion. In measurement systems, the achievable resolution may be affected by sensor characteristics, calibration errors, electronic noise, and ADC quantization [52]. Therefore, the following analysis represents the theoretical quantization-limited resolution of the sensing chain rather than the total measurement accuracy.

The pressure sensor employed in the proposed system is the MPXH6400A, which has an operating pressure range of 20–400 kPa and a nominal sensitivity of 12.1 $mV\,kPa^{-1}$. According to the manufacturer's datasheet, the sensor has a typical full-scale span of 4.6 V at a 5.0 V supply and a specified maximum accuracy error of $\pm 1.5\% V_{FSS}$, corresponding to approximately ±5.5 kPa [53]. This accuracy specification should be distinguished from the resolution of the measurement chain. Although taring the system immediately before welding can compensate for the initial output offset, other contributions to the sensor accuracy, including linearity, hysteresis, and temperature-dependent effects, may remain [53]. Accordingly, the manufacturer-specified accuracy is not treated as an additional resolution term in the following quantization analysis.

For an n_{ADC}-bit ADC with a reference voltage V_{ref}, the minimum resolvable voltage step is given by [52]

$$\Delta V_{\min} = \frac{V_{\text{ref}}}{2^{n_{\text{ADC}}} - 1} \tag{2}$$

For the 10-bit ADC used in the sensing chain and $V_{ref} = 5.0$ V, equation (2) gives a voltage resolution of approximately 4.88 mV.

Given the sensor sensitivity S_{sensor}, the corresponding minimum resolvable pressure change is expressed as

$$\Delta P_{\min} = \frac{\Delta V_{\min}}{S_{\text{sensor}}} \tag{3}$$

Using the nominal sensitivity of 12.1 mV kPa^{-1} specified for the MPXH6400A [53], the resulting pressure resolution is approximately 0.403 kPa.

Finally, the theoretical angular resolution can be estimated from the experimentally determined pressure-angle sensitivity of the system:

$$\Delta\theta_{\min} = \frac{\Delta P_{\min}}{S_{\text{sys}}} \tag{4}$$

At a shielding gas flow rate of 30 l min^{-1}, a 5° angular deviation produced a pressure change of approximately 4 kPa, corresponding to an empirical system sensitivity of $S_{\text{sys}} = 0.8$ kPa/°. Substitution into equation (4) therefore gives a theoretical angular resolution of approximately 0.5°.

This result indicates that the quantization limit of the sensing chain is approximately half of the targeted ∼1° practical resolution. The calculated value should not be interpreted as the total angular measurement accuracy, since practical performance may additionally be affected by gas-flow fluctuations, pressure fluctuations, electronic noise, sensor drift, and other sources of measurement uncertainty [52]. Nevertheless, the theoretical resolution suggests that a monitoring resolution of ∼1° may be feasible under the tested conditions.

5.2. Limitations and practical considerations

The proposed pressure-based angular monitoring approach relies on the assumption that the nozzle-to-surface (stand-off) distance remains constant, since the shielding gas exit area is a function of both the torch angle and this distance. In the present experimental and numerical framework, the stand-off distance was held fixed in order to isolate the effect of angular variation alone. In a fully free-hand welding scenario, unintended movement in the surface normal direction of the torch could alter the sensed pressure in a manner indistinguishable from an angular deviation; this coupling should therefore be regarded as a limitation of the current system. In practical implementations, the pressure sensor should be paired with a mechanism that decouples the stand-off distance from torch orientation, such as roller or skid guides that maintain a fixed working distance while still permitting angular pivoting, an approach already employed in assisted hand-held laser welding systems [6]. Alternatively, a secondary non-contact stand-off sensor could be used to compensate for distance-induced pressure variations in real time. Experimentally quantifying this coupling is left for future work.

Several aspects of the present study should be considered when generalizing the results. First, only one nozzle diameter (7 mm) and one shielding gas (argon) were investigated. Although the effect of nozzle geometry on focal-shift compensation is addressed analytically (equation (1)), its influence on pressure-angle sensitivity was not experimentally verified. Other shielding gases, such as He and CO_2, were also not considered. Second, each condition was tested with a limited number of repetitions ($n = 4$), which may limit the statistical robustness of the reported error bars. Finally, as noted above, the experimental validation was performed only under steady-state holding conditions, and the effect of dynamic torch motion was not evaluated.

6. Conclusions

This study establishes the scientific and analytical foundation for tracking manual laser welding torch orientation via nozzle-outlet shielding gas pressure. By replacing complex vision systems or inertial hardware with a straightforward pneumatic approach, the method offers a potentially simple and low-cost integration path for industrial hand-held torches. The key implications, limitations, and future directions of this work are summarized as follows:

- The numerical and experimental results show a monotonic pressure-angle relationship, and the numerical analysis indicates negligible sensitivity of the sensor reading to tool rotation (β).
- The derived closed-form empirical transfer functions avoid iterative root-finding and provide a basis for direct embedding into torch control software for future real-time angle estimation and operator feedback.
- System sensitivity is highly pronounced at steep angles and high flow rates, whereas shallow angles ($\theta > 45°$) and low flow rates yield less distinguishable signals, defining clear boundaries for the system's effective operating window.

- Beyond angular error detection, the primary shielding gas flow provides concurrent aerodynamic resistance against spatter contamination; its effects on lens replacement intervals and operating costs were not quantified in this study.
- The present framework relies on steady-state conditions with a fixed stand-off distance, a single nozzle geometry (7 mm), and pure argon, making it susceptible to distance-induced pressure fluctuations if uncoupled from mechanical skids or secondary distance sensors.
- Future work will focus on extending this static framework to dynamic welding conditions, including hand-induced tremors and continuous torch movement. The study will also be expanded to different shielding gases (He, CO_2), nozzle configurations, and combined tilt and rotation errors, with the ultimate goal of developing a real-time closed-loop control system.

Acknowledgment

This study was supported by Bursa Uludag University Research Projects Coordination Office under the Grant Number FUİ-2026-2755. The authors thank the BUU BAP Unit for its support. The authors also acknowledge TÜBİTAK (Project No. 119C115), Durmazlar Makina San. ve Tic. A.Ş., and Evinoks Servis Ekipmanları San. ve Tic. A.Ş. for their support.

Data availability statement

The data that support the findings of this study are available from the corresponding author upon reasonable request.

Conflict of interest

Murat Reis is a named inventor on patent applications WO2024005746A1 and WO2025144200A1 relating to the torch designs discussed in this article. The applications are owned by the applicant organisations, which may seek commercialisation. The authors declare no other competing interests.

Author contributions

Deniz Kaya 0000-0001-6926-8206
Conceptualization (equal), Data curation (equal), Formal analysis (equal), Resources (equal), Software (equal), Visualization (equal), Writing – original draft (equal), Writing – review & editing (equal)

Mustafa K. İşman 0009-0001-4153-088X
Data curation (equal), Formal analysis (equal), Software (equal), Writing – review & editing (equal)

Ebubekir Beyazoğlu 0000-0002-7327-8471
Data curation (equal), Investigation (equal), Software (equal), Writing – original draft (equal)

Murat Reis 0000-0001-5853-488X
Conceptualization (equal), Formal analysis (equal), Funding acquisition (equal), Methodology (equal), Project administration (equal), Supervision (equal), Writing – review & editing (equal)

References

[1] Berrizbeitia S E, Galnares I C, Egurtza A P, de Lacalle L N L and Pereira Neto O 2023 Feasibility study of handheld laser welding technology for small thickness aluminium alloys *Key Eng. Mater.* **955** 89–99
[2] Sowards J 2023 Welding in space: past, present, and future 2023 AWS Professional Program (Chicago, IL)11–14 September 2023 (NASA Technical Reports Server, Document ID 20230012815 https://ntrs.nasa.gov/citations/20230012815)

[3] Yilmaz G, Kisin B, Kaya D, Ozalp A A, Reis M and Cavdar K 2026 A parametric study on laser-assisted preheating and post-weld heat treatment to enhance the mechanical properties of aisi 1075 high-carbon steel for electric vehicle manufacturing applications *Opt. Laser Technol.* **193** 114228
[4] Reis M and Şerifağaoğlu E 2022 A smart handheld welding torch device for manual spot laser welding *Appl. Sci. (Switzerland)* **12** 11137
[5] Reis M, İrfan N C, Koyaş B, Akyüz M E and Şerifağaoğlu E 2024 Smart hand welding torch system and method for manual laser welding Patent No. WO2024005746A1.
[6] Caprio L, Borzoni G, Previtali B and Demir A G 2023 Hand-held laser welding of aisi301ln for components with aesthetic requirements: toward the integration of machine and human intelligence *J. Laser Appl.* **35** 012008
[7] Madrid J, Lorin S, Söderberg R, Hammersberg P, Wärmefjord K and Lööf J 2019 A virtual design of experiments method to evaluate the effect of design and welding parameters on weld quality in aerospace applications *Aerospace* **6** 74
[8] Salminen A, Jansson A and Kujanpää V 2003 Effect of welding parameters on high power diode laser welding of thin sheet High-Power Diode Laser Technology and Applications Proc. SPIE 4973 Zediker M S 106–15 (SPIE)
[9] Xia P, Xiong L, Hu Y, Feng X and Wang C 2023 Effect of laser oscillation and beam incident angle on porosity in double-sided filler welding of 2219 aluminum alloy t joint *Opt. Laser Technol.* **166** 109581
[10] Mei L, Yan D, Chen G, Wang Z and Chen S 2017 Influence of laser beam incidence angle on laser lap welding quality of galvanized steels *Opt. Commun.* **402** 147–58
[11] Jung S H and Kim H J 2023 Application of laser welding to STS301L side structure of railway vehicles (ii) - incidence angle welding conditions for laser beam based on multiple regression analysis of dummy variables *J. Mech. Sci. Technol.* **37** 4249–58
[12] Kumar N, Mukherjee M and Bandyopadhyay A 2017 Study on laser welding of austenitic stainless steel by varying incident angle of pulsed laser beam *Opt. Laser Technol.* **94** 296–309
[13] Palanisamy S, Rajendran R and Kumar S S 2023 Effect of incident angle on weld microstructure and mechanical properties of laser beam welded nitronic -50 austenitic stainless steel joints *Micron* **169** 103457
[14] Liao Y C and Yu M H 2007 Effects of laser beam energy and incident angle on the pulse laser welding of stainless steel thin sheet *J. Mater. Process. Technol.* **190** 102–8
[15] Balasubramanian K R, Buvanashekaran G and Sankaranarayanasamy K 2010 Modeling of laser beam welding of stainless steel sheet butt joint using neural networks *CIRP J. Manuf. Sci. Technol.* **3** 80–84
[16] Herrmann J 2011 The role of process gases in laser welding *Laser Tech. J.* **8** 24–27
[17] Schmidt L, Schricker K, Bergmann J P and Junger C 2020 Effect of local gas flow in full penetration laser beam welding with high welding speeds *Appl. Sci. (Switzerland)* **10** 1867
[18] Schmidt L, Schricker K and Bergmann J P 2021 Experimental and numerical analysis of local gas supplies for spatter reduced high speed laser beam welding *Lasers in Manufacturing Conf. 2021, (Ilmenau, Germany)*
[19] Schmidt L, Schricker K, Diegel C, Sachs F, Bergmann J P, Knauer A, Romanus H, Requardt H, Chen Y and Rack A 2024 Effect of partial and global shielding on surface-driven phenomena in keyhole mode laser beam welding *Weld. World* 68 1353–74
[20] Grevey D, Sallamand P, Cicala E and Ignat S 2005 Gas protection optimization during Nd: YAG laser welding *Opt. Laser Technol.* **37** 647–51
[21] Zhang L, Zhang J, Zhang G, Bo W and Gong S 2011 An investigation on the effects of side assisting gas flow and metallic vapour jet on the stability of keyhole and molten pool during laser full-penetration welding *J. Phys. D: Appl. Phys.* **44** 135201
[22] Xie D and Yin G 2021 Hand-held type laser welding head subassembly of blowing Patent No. CN212350766U.
[23] Watkins K G 2003 Laser welding of magnesium alloys *Magnesium Technology 2003 (TMS Annual Meeting)*, 153–6
[24] Chen A, Li B, Chen X, Jiang M, Zou S, Tao W, Lei Z and Chen Y 2023 Experimental and numerical investigation of shielding gas behaviors in laser welding of TC4 alloy *Materials* **16** 6511
[25] Ly N, Markushov I, Grapov Y, Monveldt S and Novikov S 2024 Material processing functionality in handheld laser system. US Patent Application Publication No. US20240286220A1
[26] Schmidt L, Schricker K, Diegel C and Bergmann J P 2022 Effect of local pressure distribution on spatter formation for welding high alloy steel at high welding speeds *Procedia Cirp* vol 111 (Elsevier B.V) pp 391–6
[27] Sibillano T, Ancona A, Berardi V, Schingaro E, Basile G and Lugarà P M 2006 A study of the shielding gas influence on the laser beam welding of AA5083 aluminium alloys by in-process spectroscopic investigation *Opt. Lasers Eng.* **44** 1039–51
[28] Hamadou M, Fabbro R and Caillibotte G 2004 Effect of gas shielding delivery mode on high power CO_2 laser welding *ICALEO 2004 - 23rd Int. Congress on Applications of Laser and Electro-Optics, Congress Proc.* (Laser Institute of America) pp 1–10
[29] Boughanmi C, Bannour S, Mhiri H and Bournot P 2018 Shielding gas coaxial jet pipes numerical study of a vertical laser welding process of az91 magnesium alloy *J. Appl. Fluid Mech.* **11** 79–94
[30] Shirvan A J, Choquet I and Nilsson H 2012 Numerical modelling of shielding gas flow and heat transfer in laser welding process *Proc. 5th Int. Swedish Production Symp.* pp 269–76
[31] Ahn J, He E, Chen L, Dear J and Davies C 2017 The effect of ar and he shielding gas on fibre laser weld shape and microstructure in AA 2024-T3 *J. Manuf. Process.* **29** 62–73
[32] Wang H, Shi Y, Gong S and Duan A 2007 Effect of assist gas flow on the gas shielding during laser deep penetration welding *J. Mater. Process. Technol.* **184** 379–85
[33] Fabbro R, Hamadou M, Sabatier L, Coste F, Raïssi K, Zanelli M and Delalondre C 2000 Study and optimization of shielding gas nozzle used for laser welding *ICALEO 2000: Proc. Laser Applications in the Automotive Industry Conf., Congress Proc.* (Laser Institute of America) pp C166–72
[34] Datta S, Raza M S, Muvvala G, Saha P and Pratihar D K 2023 The effect of different laser head angles and shielding gas supply systems to maximize the depth of penetration by minimizing the plasma shielding effect in fiber laser welding of 3-mm thick nitinol sheet *Optik* **283** 170903
[35] Jovic G, Bormann A, Pröll J and Böhm S 2020 Laser welding with side-gas application and its impact on spatter formation and weld seam shape *Procedia Cirp* vol 94 (Elsevier B.V.) pp 649–54
[36] Diegel C, Schricker K, Schmidt L, Dorschner D and Bergmann J P 2022 Evaluation of the effect of local gas flows on keyhole geometry by means of a half-section setup *Procedia Cirp* vol 111 (Elsevier B.V) pp 385–90
[37] Diegel C, Mattulat T, Schricker K, Schmidt L, Seefeld T, Bergmann J P and Woizeschke P 2023 Interaction between local shielding gas supply and laser spot size on spatter formation in laser beam welding of AISI 304 *Appl. Sci. (Switzerland)* **13** 10507
[38] Vyskoč M, Dománková M, Sahul M and Vyskočová M 2020 The effect of the shielding gas flow rate on the geometry, porosity, microstructure and mechanical properties of laser weld joints *Res. Pap. Fac. Mater. Sci. Technol. Slovak Univ. Technol.* **28** 72–85

[39] Yang X, Chen H, Zhu Z, Cai C and Zhang C 2019 Effect of shielding gas flow on welding process of laser-arc hybrid welding and MIG welding *J. Manuf. Process.* **38** 530–42
[40] Blackburn J, Allen C, Hilton P and Li L 2010 Nd: YAG laser welding of titanium alloys using a directed gas jet *J. Laser Appl.* **22** 71–78
[41] Reis M 2025 A welding torch that automatically adjusts the focus in manual laser welding operations Patent No. WO2025144200A1
[42] Günther J, Prowaznik R, Krug D, Jahn S, Niendorf T and Wegener T 2025 Microstructure and mechanical properties of hand-held laser beam welded S700MC high-strength steel *J. Adv. Join. Process.* **12** 100359
[43] Kumar A 2025 Exploring manual laser oscillation welding of stainless steel in different joint configurations *Lasers Manuf. Mater. Process.* **12** 1037–60
[44] Azhikannickal E, Bates P J and Zak G 2012 Use of thermal imaging to characterize laser light reflection from thermoplastics as a function of thickness, laser incidence angle and surface roughness *Opt. Laser Technol.* **44** 1491–6
[45] Jahn S, Pieper M, Schmitz M, Prowaznik R, Lange J, Wolters M, Rockser M and Kiziltas K 2026 Laser beam characteristics of handheld laser beam welding systems *Weld. World* **70** 5083–5095
[46] Menter F R 1994 Two-equation eddy-viscosity turbulence models for engineering applications *AIAA J.* **32** 1598–605
[47] Ramsey G M, Galloway A M, Campbell S W, McPherson N A and Scanlon T J 2012 A computational fluid dynamic analysis of the effect of side draughts and nozzle diameter on shielding gas coverage during gas metal arc welding *J. Mater. Process. Technol.* **212** 1694–9
[48] Haupt W, Borges L G, Israel C L and Riffel K C 2024 Effects of laser welding on the mechanical properties and microstructure of AISI 304 stainless steel *Lasers Manuf. Mater. Process.* **11** 887–904
[49] Zhang W, Xiao J, Chen H and Zhang Y 2014 Measurement of three-dimensional welding torch orientation for manual arc welding process *Meas. Sci. Technol.* **25** 035010
[50] Zhang G, Shi Y, Gu Y F and Fan D 2017 Welding torch attitude-based study of human welder interactive behavior with weld pool in GTAW *Robot. Comput.-Integr. Manuf.* **48** 145–56
[51] Suwanratchatamanee K, Yap H E, Sawada H and Hashimoto S 2025 A novel plasma cutting articulated robot system with torch angle sensor and its applications in industry *2025 IEEE Int. Conf. on Mechatronics and Automation, ICMA 2025* (Institute of Electrical and Electronics Engineers Inc) pp 222–7
[52] Northrop R B 2014 *Introduction to Instrumentation and Measurements* 3rd edn (CRC Press)
[53] NXP Semiconductors 2017 MPXH6400A, 20 to 400 kPa, absolute, integrated pressure sensor Data Sheet NXP B.V